Journal of the European Ceramic Society **18** (1998) 693–699

PII: S0955-2219(97)00192-1
0955-2219/98/$19.00 + 0.00

Microstructure and Mechanical Properties of Yttria Stabilized Zirconia/Silicon Carbide Nanocomposites

Noriko Bamba, Yong-Ho Choa, Tohru Sekino and Koichi Niihara*

The Institute of Scientific and Industrial Research, Osaka University, 8-1 Mihogaoka, Ibaraki, Osaka 567, Japan

(Received 28 July 1997; accepted 22 October 1997)

Abstract

Fully stabilized 8YSZ/SiC nanocomposites were fabricated by hot-pressing technique, and the microstructure and mechanical properties were investigated. The fine SiC particulate inhibits densification and grain growth, this is due to the decreasing grain boundary diffusivity and mobility. Compared with the monolith, the composite system possesses narrow and homogeneous grain size distribution, and this tendency becomes more obvious with increasing SiC content. The fine and homogeneous microstructure improves the fracture strength; for instance, 5 and 20 vol% SiC nanocomposites showed 580 and 750 MPa of the strength, respectively. Fracture toughness was found to be improved due to the crack deflection at the crack tip. © *1998 Elsevier Science Limited. All rights reserved*

1 Introduction

Yttria fully stabilized zirconia (YSZ) with fluorite structure is well known as a solid electrolyte that possesses high oxygen ionic conductivity over wide ranges of temperature and oxygen partial pressure, and it is widely used as an oxygen sensor and a fuel cell.[1–3] In these applications, the requirement for YSZ is not only high conductivity but also better mechanical, chemical and electrical stability in special environments. Eight mol% yttria stabilized zirconia (8YSZ) is one of the widely used materials as a solid electrolyte. However, 8YSZ is not a strong material, therefore an improvement of mechanical properties is strongly required to widen its application.

*To whom correspondence should be addressed. Fax: +81-6-879-8444.

Two major directions are applied to strengthen and toughen zirconia and other ceramics: the first is to use the phase transformation of zirconia from tetragonal to monoclinic induced by mechanical stresses,[4,5] and the second is to use the composite technology by incorporating particulate, whiskers, platelets or fibers.[6–10] Ceramic based nanocomposite is one of the particulate reinforced composites, in which the nano-sized particulate is dispersed within the matrix grains and/or at the grain boundaries. Recently various kinds of ceramic based nanocomposites in the ceramic/ceramic,[11–16] ceramic/metal[17–21] and intermetallic/ceramic[22,23] composite systems are researched. Of these nanocomposites, the oxide based nanocomposites demonstrated significantly improved mechanical properties even at high temperatures. For example, the fracture strength[11] and creep resistance[13,14] of Al_2O_3 were improved by 3 to 5 times and by 3 to 4 orders by incorporating only 5 vol% nano-sized SiC particulate, respectively.

In this study, the nanocomposite techniques were applied in order to improve the mechanical properties of fully stabilized 8YSZ. Nano-sized SiC particulate was used as a dispersion phase, because SiC has much lower thermal expansion coefficient than 8YSZ and higher Young's modulus and strength. Special emphasis has been spent to investigate microstructural characteristics and to evaluate the effects of nano-sized SiC addition on microstructure as well as mechanical property for 8YSZ/SiC nanocomposites fabricated by hot-pressing technique.

2 Experimental Procedure

8YSZ with average crystalline size of 20 nm (Sumitomo Osaka Cement Co., Ltd.) and β-SiC with average grain size of 70 nm (Mitsui Touatus

Ltd.) were used as the matrix and dispersion, respectively. 8YSZ and β-SiC powders which is 0, 5, 10 and 20 vol% with 8YSZ content were ball-milled in C_2H_5OH for 48 h. The mixed powders were dry ball-milled for 12 h after being dried in a rotational vacuum drier, and then were sieved under 150 μm to remove hard agglomerate particles. The powders were hot-pressed at 1300–1900°C for 1 h under 30 MPa in Ar atmosphere. The sintered bodies were cut and ground into rectangular bar specimens (4×3×36 mm) and polished using diamond paste with 0·5 μm to evaluate the microstructure and mechanical properties.

Relative densities of the specimens were measured by the Archimedes method using toluene. Fracture strength was measured by the 3-point bending test (specimen size: 4×3×36, span : 30 mm, crosshead speed: 0·5 mm min^{-1}). The edges of tensile surfaces were beveled at 45° to avoid the fracture from the specimen edges. Fracture toughness was evaluated from the indentation fracture (IF) method with 49 N load at room temperature.[24] The crystalline phases of each specimen were identified by X-ray diffraction (XRD) analyses with Cu Kα radiation. The microstructure investigations were performed using both scanning electron microscopy (SEM) and transmission electron microscopy (TEM). The sample surfaces for SEM observations were thermally etched in air for the monolith and Ar atmosphere for the composites at 1300–1450°C for 10 min. The samples for TEM were mechanically ground to about 150 μm thick, and were finally thinned by Ar ion beam after dimpling. Grain size and its distribution were analyzed from SEM photographs by using image analysis technique (NIH image, National Institute of Health, USA).

3 Results and Discussions

3.1 Microstructural characteristic

8YSZ monolith and 8YSZ/5–20 vol% SiC nanocomposites were fabricated by using hot-pressing technique. X-ray diffraction analysis showed that all the composites were composed of only cubic ZrO_2 and β-SiC, and free from reaction phases. Thus, the changes of microstructure and mechanical properties to be observed for 8YSZ/SiC nanocomposites should be mainly attributed to fine SiC particle dispersions.

Figure 1 shows a TEM image of the 8YSZ/5 vol% SiC composite sintered at 1700°C, and Fig. 2 presents representative SEM images of 8YSZ monolith and 8YSZ/5 vol% SiC composite sintered at 1400 and 1700°C, respectively. The TEM image indicates that SIC particulate is

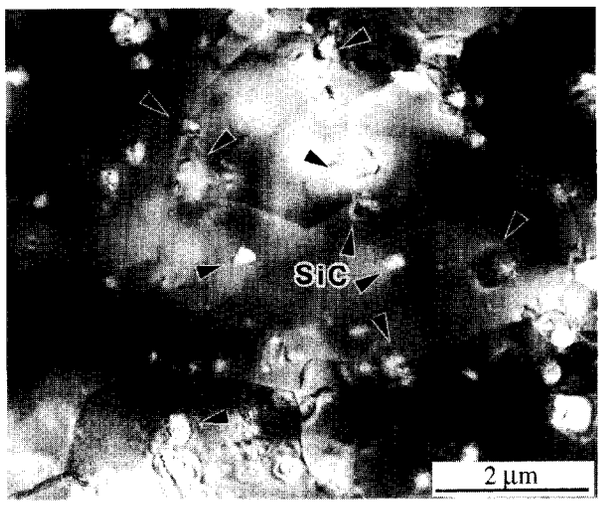

Fig. 1. TEM image of the microstructure for the 8YSZ/5 vol% SiC composite sintered at 1700°C.

homogeneously dispersed within the 8YSZ matrix grains and/or at the grain boundaries. The SiC particles with sub-micron size were mainly located at the grain boundaries, while the finer ones were within the matrix grains. Similar SEM and TEM observations were also made for the 8YSZ/20 vol% SiC composites. The observed morphologies could be explained as follows: the dispersion particles, in general, inhibit grain boundary migration of the matrix. However, for the finer SiC particles, the

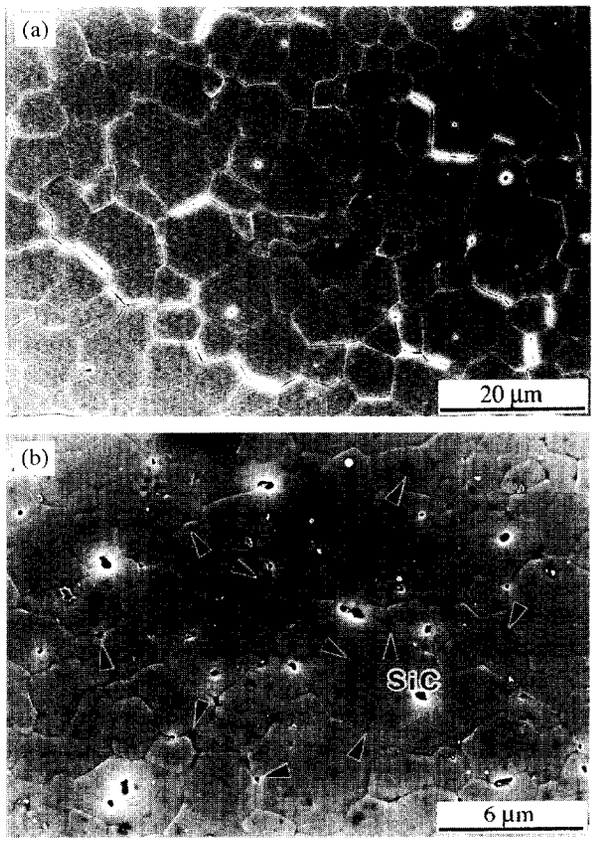

Fig. 2. SEM images of the etched surfaces for (a) the 8YSZ monolith and (b) the 8YSZ/5 vol% SiC composite sintered at 1400 and 1700°C, respectively.

matrix grain boundary can pass through the SiC particles, which are taken into the matrix grains. On the contrary, the large SiC particles remain at the grain boundaries without being taken into the matrix grain, because the grain boundary cannot pass through the larger SiC particulate such as submicron particles. This behavior is attributed to the interaction between the pinning force by one particle and the driving force for grain boundary migration.[25,26] It is evident from SEM images in Fig. 2 that grain boundary migration is inhibited by SiC particles. As shown in Fig. 2(b), the distorted grain boundaries of the 8YSZ matrix were observed in the 8YSZ/SiC composite and the SiC particles were located at the grain boundaries, while grain boundaries of 8YSZ monolith were almost straight as seen in Fig. 2(a).

Figure 3 shows the variation of relative density with sintering temperature for the 8YSZ monolith and 8YSZ/SiC nanocomoposites. Higher sintering temperatures are necessary to densify the mixed powders incorporating fine SiC particles, compared with the monolith, for instance, 1600 and 1800°C are required for 5 and 20 vol% SiC nanocomposites, respectively, to obtain over 99% of the theoretical density. The temperature which green body was just fully densified should be a critical temperature of densification. The critical temperature is higher with increasing SiC content.

These results indicate that the decrease of densification is due to the fine SiC particulate addition into the 8YSZ matrix. Some explanation for the retardation of densification in this system could be suggested. The distribution of SiC particulate with an extreme difficulty in densification will decrease the sintering rate by inducing tensile mean stress which is developed by the differential shrinkage characteristics between 8YSZ matrix and SiC dispersion.[27]

In addition, grain boundary diffusivity should be decreased by the SiC addition.[25] As well known, the grain boundary diffusion is the predominant mechanism of matter transport.[28] When SiC particulate is located at the grain boundaries as shown in Figs 1 and 2, the grain boundary diffusion path becomes longer in proportion to the diameter of the SiC particulate, and the diffusion of atoms/vacancies along the interface between 8YSZ grain and SiC particle should be slower. The observed retardation of densification, therefore, is due to the decrease in the grain boundary diffusivity which results from the SiC dispersion. Therefore, in the composites case, higher temperature for densification might be necessary to supplement the decrease in the diffusivity, compared with the monolith.

After densified, the decrease in the density was observed only for monolith sintered at 1600°C. This is due to the trapping of pores into matrix grain at higher sintering temperature, because the mobility for grain boundary is larger than that for pore in monolithic case.[29,30] For 5 and 20 vol% SiC dispersed nanocomposites, however, intragranular-pore was not observed, because the grain boundary mobility is decreased by the SiC fine particles which pin the grain boundary movement.

The grain boundary mobility also influences grain growth as well as densification.[25] Fig. 4(a) and (b) show the relationship between sintering temperature and mean grain size of matrix, and the

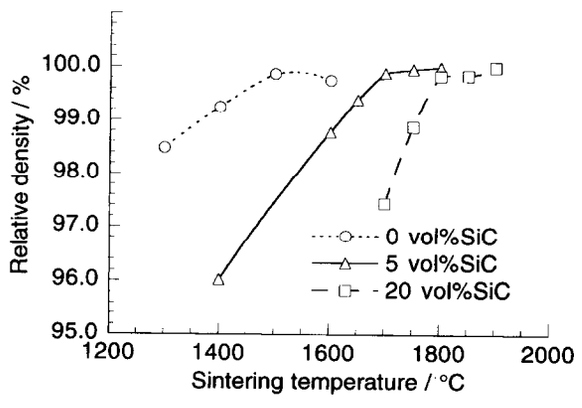

Fig. 3. The variation of relative density with sintering temperatures for 8YSZ monolith, 8YSZ/5 vol% SiC and 8YSZ/20 vol% SiC composites.

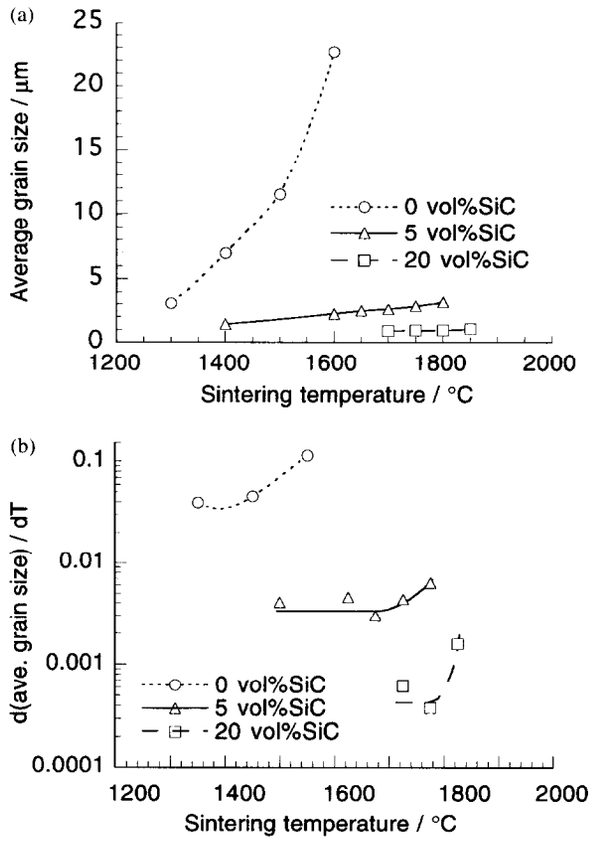

Fig. 4. (a) The mean grain size with sintering temperatures and (b) its differential graph for 8YSZ monolith, 8YSZ/5 vol% SiC and 8YSZ/20 vol% SiC composites.

change of the mean grain size with the temperature (dG/dT), respectively. The mean grain size of 8YSZ monolith became larger and grain growth rapidly progressed with increasing sintering temperature. For nanocomposites, grain growth of 8YSZ matrix decreased by fine SiC particle dispersion, and dG/dT of nanocomposites are smaller than that of monolith. For example, the grain size of monolith sintered at 1600°C was about 23 μm and that of the 5 vol% SiC nanocomposite at 1600°C was only 2 μm. Minimum dG/dT value of each composite depends on composition, judging from Fig. 4(b), the degree of increment for composites reduced. Therefore, it seems to be difficult to make densified body with fine grain size for monolith, due to higher grain growth with temperature as shown in Fig. 4(b). The matrix grain growth with the temperature of nanocomposites is significantly inhibited by addition of SiC particulate, whose microstructure become finer. This is attributed to the decrease of the grain boundary mobility and diffusivity as well as densification. Judging from Figs 3 and 4(b), the temperature at which the sample is fully densified is almost similar to the temperature at which the dG/dT rapidly increase, and the dG/dT decreases with increasing the second phase content.

The dependence of the grain size on the second phase content can be explained by using Zener's equation which suggests a relationship between grain size of matrix and volume fraction and particle size of the second phase.[31]

$$G = k(r/f) \tag{1}$$

where G, k, r and f are mean grain size of matrix, constant, mean grain size of second phase and volume fraction of second phase, respectively. Equation (1) shows that the grain size of matrix depends on particle size and volume fraction of second phase. Equation (1) clearly suggests that mean grain size (G) decreases with increasing volume fraction (f) of SiC.

Grain size distributions for the sintered bodies around the critical temperature judging from the results of the density and dG/dT are shown in Fig. 5. The 8YSZ monolith sintered at 1400°C displays the wide grain size distribution from 1

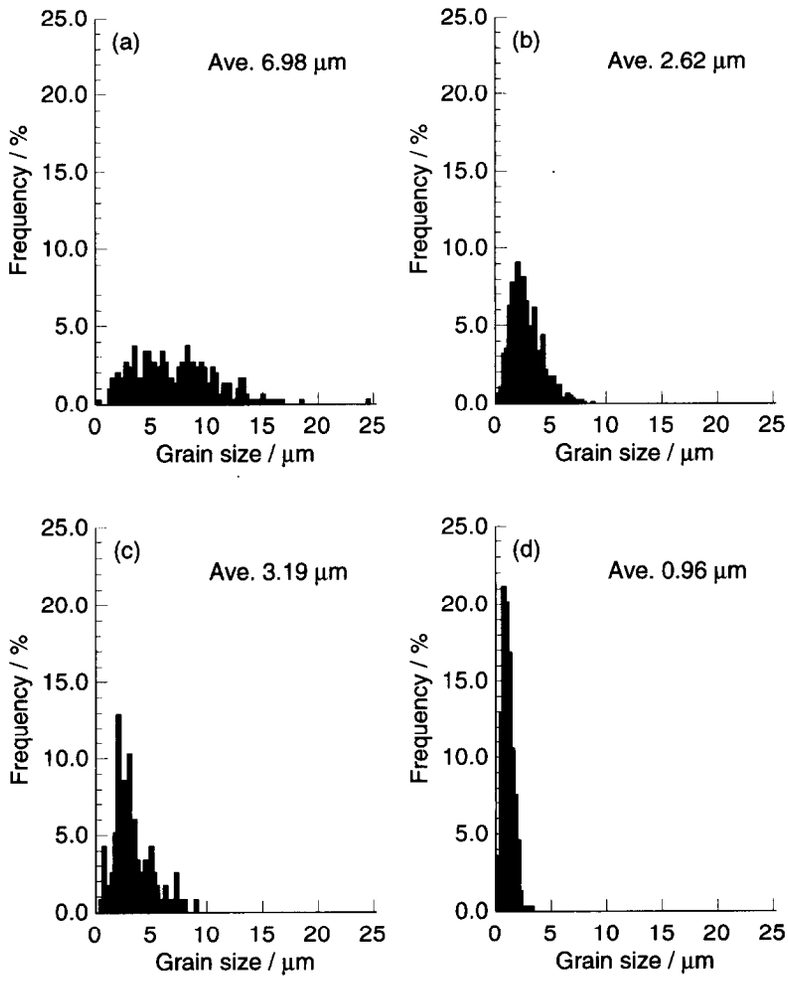

Fig. 5. The grain size distribution for (a) 8YSZ monolith sintered at 1400°C, (b) 8YSZ/5 vol% SiC composite at 1700°C, (c) 8YSZ/5 vol% SiC composite at 1800°C and (d) 8YSZ/20 vol% SiC composite at 1800°C.

to 25 μm, while nanocomposite systems indicate the narrow distribution even though sintering temperature is higher than the monolith. The maximum grain size for 5 vol% SiC nanocomposite sintered at 1700°C is below 10 μm. The grain growth with higher sintering temperature decreases in 20 vol% SiC composite system, and maximum grain size is under 3 μm even at 1800°C of sintering temperature. Nanocomposite systems possess narrow and homogeneous grain size distribution by fine SiC additions.

Consequently, both the densification and grain growth are inhibited by SiC particle addition into 8YSZ, as reported by several researchers for other composites system.[25,26,32,33] On the other hand, in order to obtain the finer and more homogeneous microstructure, finer SiC particle dispersion are more effective, because finer SiC dispersion drastically depress the normal/abnormal grain growth.

3.2 Mechanical properties

Each fracture strength for the monolith, 5 and 20 vol% SiC composites is depicted in Fig. 6. The fracture strength of 8YSZ was remarkably improved by incorporating SiC particles. The monolithic 8YSZ sintered at 1400°C exhibited a maximum strength of 300 MPa, while the maximum strength of 5 and 20 vol% SiC composites are 580 and 750 MPa, respectively. Sintering temperature of each composite is 1700 and 1850°C. Each sintering temperature exhibited maximum strength was similar to the temperature at which the green body was just densified and the dG/dT rapidly increase as shown in Fig. 4(b). Therefore it is evident that microstructure greatly affects the mechanical properties such as fracture strength and this improvement may be attributed to following reasons. The first is the refinement of the matrix grain size. Mean grain size of monolithic 8YSZ sintered at 1400°C was 7 μm, while nanocomoposites dispersed 5 and 20 vol% SiC were 3 and 1 μm, respectively, even though they were sintered at higher temperatures such as 1700 and 1850°C than the monolith as shown in Fig. 4. From Fig. 5, the homogeneity in the matrix grain size distribution is given as a second reason. Figure 7 shows the relationship between maximum grain size and fracture strength. Densified monolith, 5 and 20 vol% SiC composites show that the strength is proportional to (maximum grain size)$^{-1/2}$, so that the improvement of strength must be due to the fine and homogeneous microstructure by SiC addition.

In addition, the increase of Young's modulus affects the improvement, which is due to addition of SiC particulate with higher Young's modulus than 8YSZ, and it can be explained by using the rule of mixture.

The fracture strength is found to be proportional to the fracture toughness as mentioned in Griffith's theory,[34] thus the fracture toughness should be the third reason of the remarkable improvement of the strength. Figure 8 indicates the variation of fracture toughness (K_{IC}) with sintering temperature. K_{IC} increased slightly with the increase of SiC content, and were 2·0, 2·2 and 2·6 MPam$^{1/2}$ for

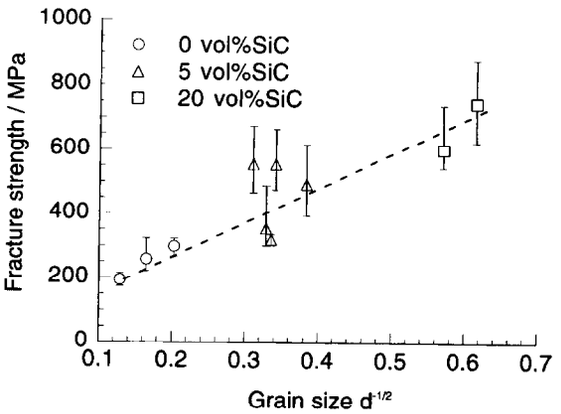

Fig. 7. The relationship between $d^{-1/2}$, where d is the maximum grain size, and fracture strength for 8YSZ monolith, 8YSZ/5 vol% SiC and 8YSZ/20 vol% SiC composites.

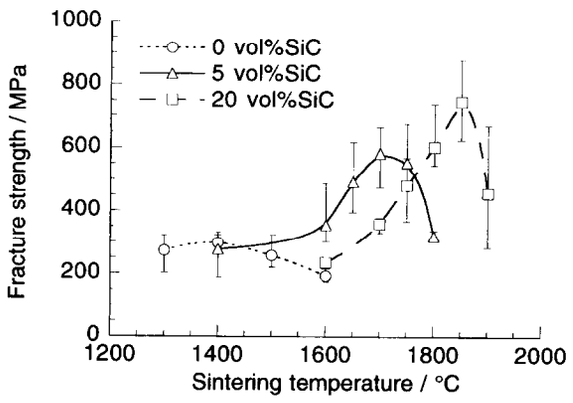

Fig. 6. The fracture strength as a function of sintering temperature for 8YSZ monolith, 8YSZ/5 vol% SiC and 8YSZ/20 vol% SiC composites.

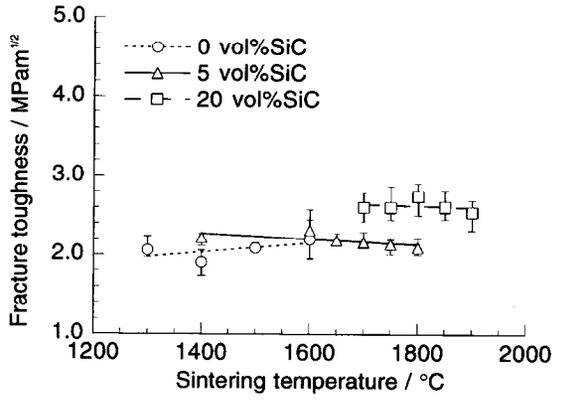

Fig. 8. The fracture toughness as a function of sintering temperature for 8YSZ monolith, 8YSZ/5 vol% SiC and 8YSZ/20 vol% SiC composites.

monolith and 5 and 20 vol% SiC nanocomposites, respectively. Generally, the increase of fracture toughness can be attributed to the crack deflection at crack tip, bowing and bridging at process zone wake by second phase.[35,36] In this system, the crack propagated straight through the 8YSZ grains for monolith, while it was deflected by SiC particle for the 20 vol% SiC nanocomoposite, as shown in Fig. 9. Therefore crack deflection may contribute to the K_{IC} improvement in the composites. Faber *et al.*[37] reported the theoretical prediction of improvement K_{IC} only by deflection for various shapes of dispersion phase. According to their results, the toughness increment can be estimated about 20% for 20 vol% SiC composite when SiC particulate is dispersed as a second phase under the assumption that the model for calculation has uniform particle spacing and no crack penetrates into dispersion particles. Theoretical and experimental K_{IC} are shown in Fig. 10, and the experimental results agreed well with the theoretical one. The improvement K_{IC} observed in this work should be mainly caused by the deflection at crack tip due to SiC particles. The deflection may be caused as a result of the residual stresses associated with differential Young's modulus and the coefficients of thermal expansion.

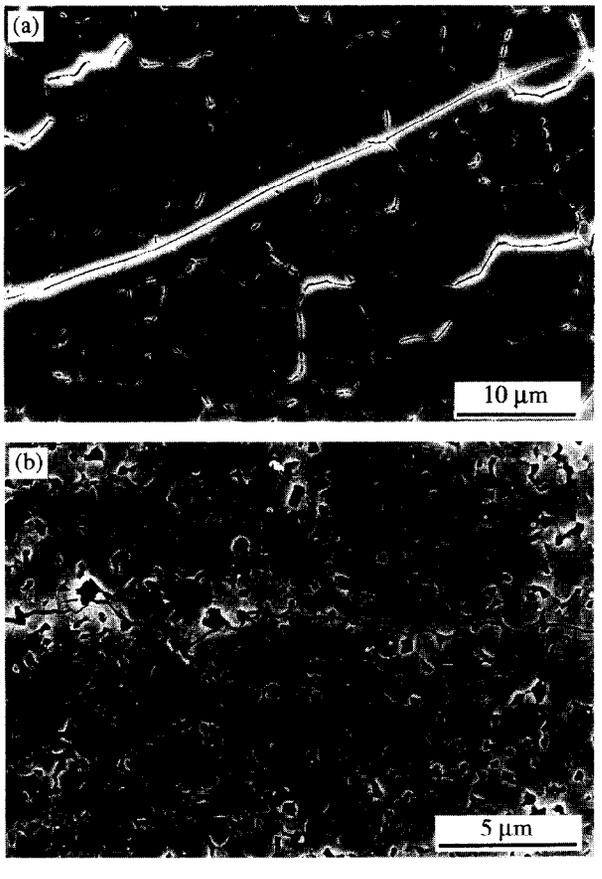

Fig. 9. SEM images of the crack deflection for (a) the 8YSZ monolith sintered at 1400°C and (b) the 8YSZ/20 vol% SiC composite sintered at 1800°C, respectively.

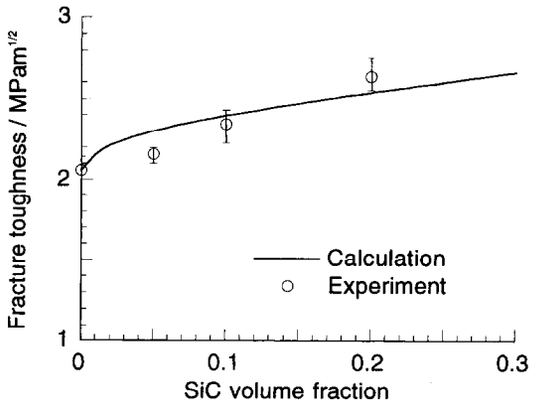

Fig. 10. The theoretical fracture toughness improved by crack deflection due to second phase and the experimental fracture toughness with SiC content. The solid line and open circle are theoretical and experimental toughness, respectively.

4 Conclusions

The 8YSZ-based nanocomposites incorporating fine SiC particulate were fabricated by using hot-pressing technique, and the effects of SiC addition on the microstructure and mechanical properties were investigated. It is difficult to fabricate 8YSZ monolith with fine microstructure because of the rapid grain growth; however, grain size of 8YSZ matrix was successively decreased by addition of SiC particulate. The composites have fine and homogeneous microstructure, which causes dominant improvement of fracture strength. The strength of the 20 vol% SiC nanocomposite up to 750 MPa. In addition, fracture toughness is also improved due to the crack deflection at the crack tip.

References

1. Saito, Y., Electrical conduction of stabilized zirconia and oxygen sensor. In *Zirconia Ceramics 1*, ed. S. Somiya. Uchida Rokakuho, Tokyo, 1983, pp. 109–125.
2. Baumard, J. F., Cales, B. and Anthony, A. M., Stabilized zirconia: basic science and applications. In *Zirconia Ceramics 1*, ed. S. Somiya. Uchida Rokakuho, Tokyo, 1983, pp. 127–144.
3. Takeuchi, M., O_2 sensor. *Bull. Ceram. Soc. Jpn.*, 1982, **17**, 433–438.
4. McMeeking, R. M. and Evans, A. G., Mechanics of transformation-toughening in brittle materials. *J. Am. Ceram. Soc.*, 1982, **65**, 242–246.
5. Marshall, D. B., Strength characteristics of transformation-toughened zirconia. *J. Am. Ceram. Soc.*, 1986, **69**, 173–180.
6. Claussen, N., Fracture toughness of Al_2O_3 with an unstabilized ZrO_2 dispersed phase. *J. Am. Ceram. Soc.*, 1976, **59**, 49–51.
7. Dougherty, S. E., Nieh, T. G. and Wadsworth, J., Mechanical properties of a 20 vol% SiC whisker-reinforced, yttria-stabilized, tetragonal zirconia composite at elevated temperature. *J. Mater. Res.*, 1995, **10**, 113–118.
8. Claussen, N., Weisskopf, K.-L. and Rühle, M., Tetragonal zirconia polycrystals reinforced with SiC whiskers. *J. Am. Ceram. Soc.*, 1986, **69**, 288–292.

9. Miao, X., Lee, W. E. and Rainforth, W. M., Pressureless sintering of zirconia–SiC platelet composites. *Br. Ceram. Trans.*, 1994, **93**, 119–125.
10. Lee, H. L. and Lee, H. M., Effect of SiC on the mechanical properties of 3Y-TZP/SiC composites. *J. Mater. Sci. Let.*, 1994, **13**, 974–976.
11. Niihara, K., Nakahira, A., Uchiyama, T. and Hirano, T., High-temperature mechanical properties of Al_2O_3–SiC composites. In *Fracture Mechanics of Ceramics*, Vol. 7, ed. R. C. Bradt, A. G. Evans, D. P. H. Hasselman and F. F. Lange. Plenum Press, New York, 1986, pp. 103–116.
12. Niihara, K., New design concept of structural ceramics–ceramic nanocomposites. *J. Ceram. Soc. Jpn.*, 1991, **99**, 974–982.
13. Nakahira, A. and Niihara, K., Microstructures and fracture behaviors at high temperatures for Al_2O_3–SiC nanocomposites. In *Fracture Mechanics of Ceramics*, Vol. 9. ed. M. Sasaki, R. C. Bradt, D. P. H. Hasselman and D. Munz. Plenum Press, New York, 1992, pp. 165–178.
14. Ohji, T., Nakahira, A., Hirano, T. and Niihara, K., Tensile creep behavior of alumina/silicon carbide nanocomposite. *J. Am. Ceram. Soc.*, 1994, **77**, 3259–3262.
15. Hirano, T. and Niihara, K., Microstructure and mechanical properties of Si_3N_4/SiC nanocomposites fabricated from amorphous Si–C–N precursor powders. *Nanostruct. Mater*, 1995, **5**, 808–818.
16. Ohji, T., Hirano, T., Nakahira, A. and Niihara, K., Particle/matrix interface and its role in creep inhibition in alumina/silicon carbide nanocomposites. *J. Am. Ceram. Soc.*, 1996, **79**, 35–45.
17. Sekino, T., Nakahira, A., Nawa, M. and Niihara, K., Fabrication of Al_2O_3/W nanocomposites. *J. Jpn. Soc. Powder. Metall.*, 1991, **38**, 326–330.
18. Nawa, M., Sekino, T. and Niihara, K., Fabrication and mechanical behaviour of Al_2O_3/Mo nanocomposites. *J. Mater. Sci.*, 1994, **29**, 3185–3192.
19. Sekino, T., Nakajima, T., Ueda, S. and Niihara, K., Reduction and sintering of a nickel- dispersed-alumina composite and its properties. *J. Am. Ceram. Soc.*, 1997, **80**, 1139–1148.
20. Sekino, T. and Niihara, K., Microstructural characteristics and mechanical properties for Al_2O_3/metal nanocomposites. *Nanostruct. Mater.*, 1995, **6**, 663–666.
21. Nawa, M., Yamazaki, K., Sekino, T. and Niihara, K., Microstructure and mechanical behaviour of 3Y-TZP/Mo nanocomposites possessing a novel interpenetrated intragranular microstructure. *J. Mater. Sci.*, 1996, **31**, 2849–2858.
22. Nakahira, A., Tamada, H. and Niihara, K., Microstructure and mechanical properties of Ti–Al based composites. *J. Jap. Soc. Powder Powder Metall.*, 1994, **41**, 514–517.
23. Suzuki, Y., Sekino, T. and Niihara, K., Effects of ZrO_2 addition on microstructure and mechanical properties of $MoSi_2$. *Scripta Metall. et Mater.*, 1995, **33**, 69–74.
24. Niihara, K., Morena, R. and Hasselman, D. P. H., Evaluation of K_{IC} of brittle solids by the indentation method with low crack-to-indent ratios. *J. Mater. Sci. Let.*, 1982, **1**, 13–16.
25. Nakahira, A. and Niihara, K., Sintering behavior and consolidation process for Al_2O_3/SiC nanocomposites. *J. Ceram. Soc. Jpn.*, 1992, **100**, 448–453.
26. Stearns, L. C. and Harmer, M. P., Particle-inhibited grain growth in Al_2O_3/SiC: I, Experimental results. *J. Am. Ceram. Soc.*, 1996, **79**, 3013.
27. Hsueh, C., Evans, A. G. and McMeeking, M., Influence of multiple heterogeneities on sintering rates. *J. Am. Ceram. Soc.*, 1986, **69**, C64–66.
28. Burke, J. E., Role of grain boundaries in sintering. *J. Am. Ceram. Soc.*, 1957, **40**, 80–85.
29. Mizutani, N., Kimura, T., Ozaki, Y. and Yamaguchi, T., Ceramic processing. In *Ceramic Science Series*, Vol. 8, ed. T. Yamaguchi and H. Yanagida. Gihodo-Shuppan Co. Ltd., Tokyo, 1985, pp. 178–179.
30. Kwon, S. T., Kim, D. Y., Kang, T. K. and Yoon, D. N., Effect of sintering temperature on the densification of Al_2O_3. *J. Am. Ceram. Soc.*, 1987, **70**, C69–70.
31. Porter, D. A. and Easterling, K. E., *Phase Transformations in Metals and Alloys*, 2nd edn. Chapman and Hall, London, 1992, pp. 139–142.
32. Okada, K. and Sukuma, T., The role of Zener's pinning effect on the grain growth in Al_2O_3–ZrO_2. *J. Ceram. Soc. Jpn.*, 1992, **100**, 382–386.
33. Mori, M., Abe, T., Itoh, H., Yamamoto, O., Takeda, Y. and Kawahara, T., Cubic stabilized zirconia and alumina composites as electrolytes in planar type solid oxide fuel cells. *Solid State Ionics*, 1994, **74**, 157–164.
34. Kingery, W. D., Bowen, H. K. and Uhlmann, D. R., *Introduction to Ceramics*, 2nd edn. John Wiley and Sons, New York, 1976, pp. 783–790.
35. Marshall, D. B. and Evans, A. G., The influence of residual stress on the toughness of reinforced brittle materials. *Mater. Forum*, 1988, **11**, 304–312.
36. Rühle, M. and Evans, A. G., High toughness ceramics and ceramic composites. *Prog. Mater. Sci.*, 1989, **33**, 85–167.
37. Faber, K. T., Evans, A. G. and Drory, M. D., A statistical analysis of crack deflection as a toughening mechanism in cerarnic materials. In *Fracture Mechanics of Ceramics*, Vol. 6, ed. R. C. Bradt, A. G. Evans, D. P. H. Hasselman and F. F. Lange. Plenum Press, New York, 1983, pp. 77–91.